Bulk photovoltaic effect in hexagonal $LuMnO_3$ single crystals

Yunwei Sheng[1], Ignasi Fina[1,*], Marin Gospodinov[2], Aaron Schankler[3], Andrew M. Rappe[3], Josep Fontcuberta[1,†]

[1]*Institut de Ciència de Materials de Barcelona (ICMAB-CSIC), Campus UAB, Bellaterra 08193, Catalonia, Spain*

[2]*Institute of Solid State Physics, Bulgarian Academy of Sciences, 1784 Sofia, Bulgaria*

[3]*Department of Chemistry, University of Pennsylvania, Philadelphia, PA 19104-6323, USA*

Supplemental Material

S-1. Normalization of the angular dependence of short circuit current

Main manuscript Fig. 2(a) is obtained by subtracting the slope extracted by points at φ = 90° and φ = 270° of the raw data in Fig S1(a), because the conditions (polarization and intensity) of light and also the J_{sc} values at any two points shifted by 180° should be the same, if there is no deviation of plate fast axes or misalignments of optical setups. This slope exists due to small laser misalignments that result in a small variation of the light intensity while rotating φ, which results in a variation of the background current. The slope-subtracted result is shown in Fig. S1(b)

Based on Eq. [7], at φ = 90°, J_{sc} (= $I_0 \alpha G_{31}$+ J_{diff} + J_{drift}) should be constant and irrelevant to θ, thus Fig S1(c) is obtained by vertical shifting the data in Fig S1(b) with reference to J_{sc}(φ = 90°, θ = 0°). In Fig. S1(d) the original J_{sc}(φ = 90°, θ = 0°) before subtraction is plotted as a function of the $\sin^2\theta$. This value is expected to be constant for any $\sin^2\theta$ value, as mentioned. In Fig. S1(e), the value of the light fluency as a function $\sin^2\theta$ is also plotted. It can be observed that the trend in Figs. S1(d,e) are similar pointing to the fact that the found variations on J_{sc}(φ = 90°, θ = 0°) result from unavoidable variation of effective light fluency in different experimental set-up at each incidence. The small discrepancy between Figs. S1(d,e) results from the intrinsic error present in the measurement of the laser fluency. The perpendicular $\alpha_\perp$ at φ = 90° is considered as constant with increasing θ.

Similarly, the V_{oc} values in Fig 2(b) are also normalized to overlap at φ = 90° with reference to J_{sc}(φ = 90°, θ = 60°).

*ifina@icmab.es

†fontcuberta@icmab.cat

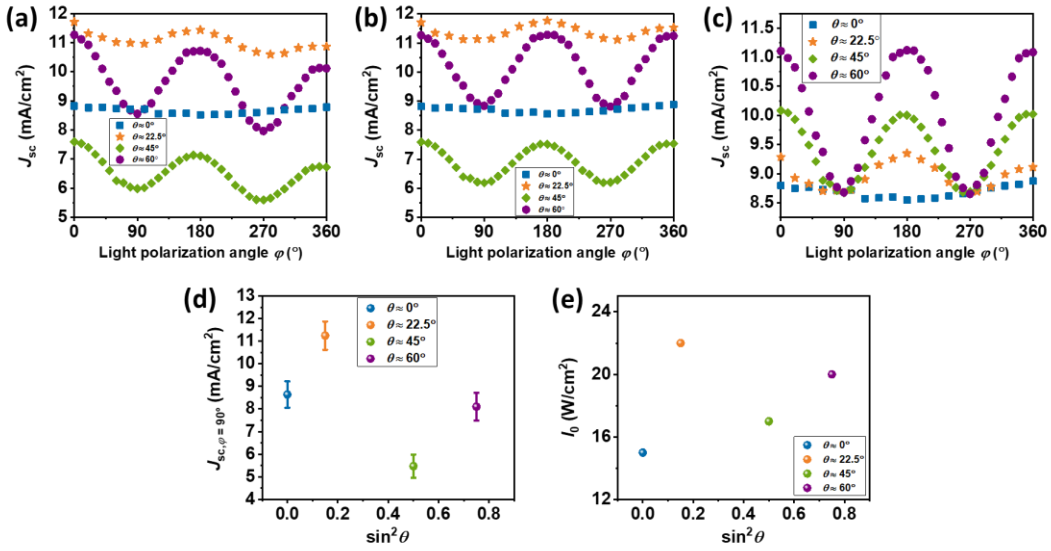

FIG. S1. The (a) raw data of $J_{sc}(\theta, \varphi)$, (b) slope subtracted $J_{sc}(\theta, \varphi)$ and (c) vertical shifted $J_{sc}(\theta, \varphi)$ with respect to $J_{sc}(\varphi = 90°, \theta = 90°)$, respectively, along the *z*-axis versus the polarization angles (φ) of the light at different incident angles, of Cry-1. Dependence of the (d) raw data of $J_{sc}(\theta, \varphi = 90°)$ and (e) light intensity I_0 reached to the crystal on $\sin^2(\theta)$. Error bars in Fig. S1(d) indicate the spread of values (SD) from data recorded in 6 junctions.

S-2 Rectifying response of the Pt/LMO/Pt device

Fig. S2 show the *J*-*V* of the Pt/LMO/Pt device. It can be observed that for negative bias the current is larger. This is expected for a p-type/metal junction. Thus, LMO acts as a p-type semiconductor as expected [1]. This disregards the important contribution of the Pt bottom electrode, which covers the whole crystal back surface.

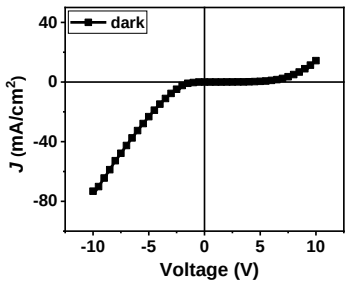

FIG. S2. *J*-*V* curves of Cry-1 in dark.

S-3 Derivation of $J_{BPE}(\theta, \varphi)$ in a non(weak)-absorbing material with *P*6$_3$cm symmetry

The dependence of the J_{sc} on the light polarization is a fingerprint of a contribution of the bulk photovoltaic effect (BPE) to the short-circuit photocurrent. In the BPE scenario, the short circuit photocurrent effect ($J_{sc,BPE}$) is given by Eq. [4], here repeated for convenience as Eq. [S3.1]:

$$J_{\mathrm{BPE,i}} = I_0 \cdot \alpha_{\mathrm{jk}} \cdot G_{\mathrm{ijk}} \cdot e_{\mathrm{j}} e_{\mathrm{k}} = I_0 \cdot \beta_{\mathrm{ijk}} \cdot e_{\mathrm{j}} e_{\mathrm{k}} \qquad [S3.1]$$

For *h*-LMO (space group $P6_3cm$), assuming a relatively weak absorption anisotropy (i.e., $\alpha_{jk} \approx \alpha$) and an uniform absorption in the crystal [10], Eq. [S3.1] can be written as:

$$\begin{pmatrix} J_x \\ J_y \\ J_z \end{pmatrix} = I_0 \begin{pmatrix} 0 & 0 & 0 & 0 & \beta_{15} & 0 \\ 0 & 0 & 0 & \beta_{15} & 0 & 0 \\ \beta_{31} & \beta_{31} & \beta_{33} & 0 & 0 & 0 \end{pmatrix} \begin{pmatrix} e_x^2 \\ e_y^2 \\ e_z^2 \\ e_y e_z \\ e_z e_x \\ e_x e_y \end{pmatrix} =$$

$$I_0 \alpha \begin{pmatrix} G_{15} e_z e_x \\ G_{15} e_y e_z \\ G_{31} e_x^2 + G_{31} e_y^2 + G_{33} e_z^2 \end{pmatrix} \qquad \text{[S3.2]}$$

where ($e_{x,y,z}$) are the components of the light polarization incoming along *k*. (Fig. 1(b)). In our experimental arrangement (Fig. 1): $\boldsymbol{e_x} = \sin(\varphi)$, $\boldsymbol{e_y} = \cos(\varphi)\cos(\theta)$ and $\boldsymbol{e_z} = \cos(\varphi)\sin(\theta)$, thus BPE (Eq. [S3.2]) predicts an angular and polarization dependence of $J_{sc,BPE}$ (θ, φ) given by

$$\begin{pmatrix} J_x \\ J_y \\ J_z \end{pmatrix} = I_0 \alpha \begin{pmatrix} \frac{1}{2} G_{15} \sin\theta \sin 2\varphi \\ \frac{1}{4} G_{15} \sin 2\theta \, (1 + \cos 2\varphi) \\ \frac{G_{33} - G_{31}}{2} \sin^2\theta \cos 2\varphi + \frac{G_{33} - G_{31}}{2} \sin^2\theta + G_{31} \end{pmatrix} \qquad \text{[S3.3]}$$

According to Eq. [S3.3] $J_{sc,BPE}$ along the *z*-axis has a cos(2φ) as

$$J_{\mathrm{BPE}} = I_0 \alpha \left(\frac{G_{33} - G_{31}}{2} \sin^2\theta \cos 2\varphi + \frac{G_{33} - G_{31}}{2} \sin^2\theta + G_{31} \right) \qquad \text{[S3.4]}$$

S-4. In-plane illumination J_{sc} (φ) measurements

In Fig. S4 (a), the J_{sc} (φ) dependence for in-plane illumination of bare and capped electrode is shown. The brown circles display the photocurrent measured using the bare A_2 = 0.37 mm^2 electrode (as in main text), while the red circles depict the photocurrent measured after capping the A_2 = 0.37 mm^2 top electrode by suitable photoabsorbing cover (even though the perfect overcover cannot be assured). It can be appreciated that the measured photocurrent is basically constant, as expected from exclusively lateral illumination.

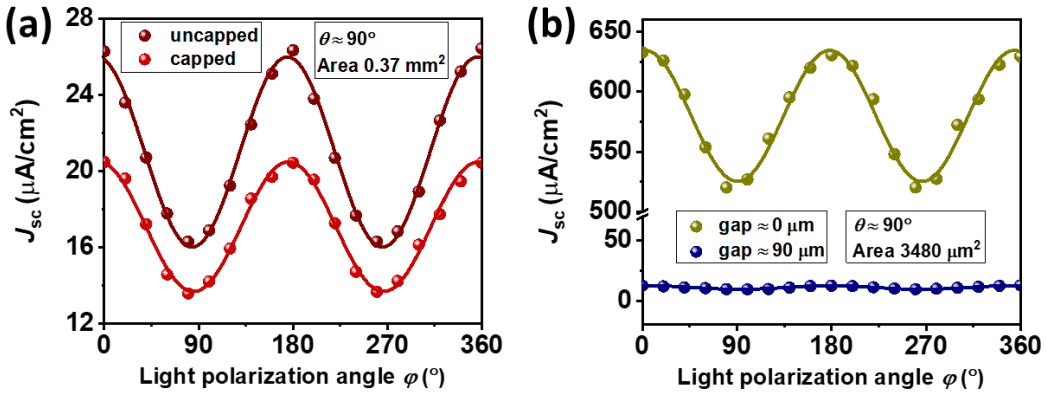

FIG. S4. (a) Dependence of the short circuit photocurrent on polarization angles (φ) of the light with in-plane incidence ($\theta \approx 90°$, Cry-3) of uncapped and capped top electrode with gap $D = 0$. (b) Dependence of the short circuit photocurrent of the light with in-plane incidence ($\theta \approx 90°$, Cry-4) on the distance of electrodes to the sample edge. Solid lines are fits using Eq. [1] of experimental data (symbols). Light intensity I_0 after optical plates is around 27.6 W/cm^2.

In Fig. S4 (b), the J_{sc} (φ) dependence for in-plane illumination with different edge-electrode distance (gap D) is shown. It can be seen that the photocurrent measured with a 90 μm gap is near zero. This results from the fact that the photocarrier generation is limited to a narrow region of depth < 1 μm and recombination limits charge extraction at distant electrodes. Note that here the absolute photocurrent is around 3 - 4 times smaller than that of Fig. 5. Using Eqs. [S5.10] and J_{sc} ($\theta \approx 90°$; φ) data of Fig. S4(b) collected for 0 gap [J_{sc} ($\theta \approx 90°$; $\varphi = 0°$) ≈ 635 μA/cm^2, J_{sc} ($\theta \approx 90°$; $\varphi = 90°$) ≈ 520 μA/cm^2, $S_1 = S_2 \approx 59$ μm, $I_0 \approx 27.6$ W/cm^2], Glass coefficients (upper bounds) $G_{31} \approx 1112$ pm/V and $G_{33} \approx 1357$ pm/V are obtained. These values are comparable with the in-plane SA case in the main manuscript.

S-5. Derivation of $J_{BPE}(\theta, \varphi)$ in an anisotropic strongly absorbing material with $P6_3cm$ symmetry

We attempt in the following to derive the BPE response of $LuMnO_3$ by taking into account the strong anisotropic (dichroism) of $LuMnO_3$.

For uniaxial system along the z-axis, optical absorption is given by:

$$\alpha_{\perp} = \frac{2\kappa_{\perp}\omega}{c} = \frac{4\pi\kappa_{\perp}}{\lambda};\ \alpha_{\parallel} = \frac{2\kappa_{\parallel}\omega}{c} = \frac{4\pi\kappa_{\parallel}} \qquad [S5.1]$$

where $\alpha_{\perp}$ and $\alpha_{\parallel}$ denote the absorption for the different component of the light electric field, namely: $\overrightarrow{E}(//x)$ (and $\vec{E}(//y)$) and $\vec{E}(//z)$, respectively.

In general, ($\overrightarrow{e_{x,y,z}}$) are the components (unit vectors) along x,y,z-axes of the polarization of light of amplitude $|E_0|$ incoming along $\boldsymbol{k}$, that will suffer different absorption. In our experimental arrangement (Fig. S5.1).

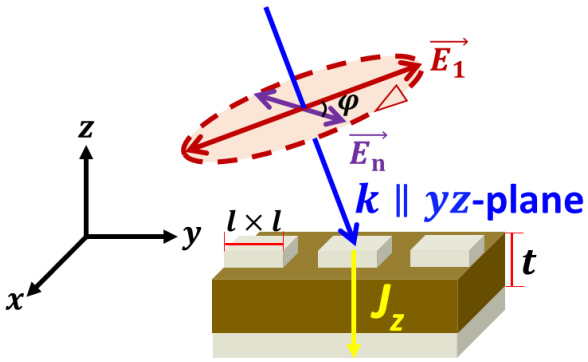

FIG. S5.1. Sketch illustrates the experimental arrangement of oblique incidence (θ). The length of the top electrode square (l x l) is $l \approx 58$ μm; the thickness of the crystal is $t \approx 100$ μm.

$$\overrightarrow{e_1} = \overrightarrow{e_x}|E_0|\sin\varphi\, e^{-\left(\frac{\alpha_\perp x}{2}\right)} e^{i(\boldsymbol{kr}-\omega t)} \qquad [S5.2]$$

$$\overrightarrow{e_2} = \overrightarrow{e_y}|E_0|\cos\varphi\cos\theta\sin\varphi\, e^{-\left(\frac{\alpha_\perp y}{2}\right)} e^{i(\boldsymbol{kr}-\omega t)} \qquad [S5.3]$$

$$\overrightarrow{e_3} = \overrightarrow{e_z}|E_0|\cos\varphi\sin\theta\sin\varphi\, e^{-\left(\frac{\alpha_\parallel z}{2}\right)} e^{i(\boldsymbol{kr}-\omega t)} \qquad [S5.4]$$

In the present case, having $LuMnO_3$ a strong absorption, $\left|E_{x,y,z}(r)\right| = g(\theta,\varphi)|E_0|e^{-\left(\frac{\alpha_{\parallel,\perp} r}{2}\right)}$ with the angular dependence $g(\theta,\varphi)$ identified in [S5.1-3], becomes a function of penetration depth. Therefore, the Eq [S3.2] needs to be modified by explicitly expressing the depth-dependence of the light intensity.

$$\begin{pmatrix} J'_x \\ J'_y \\ J'_z \end{pmatrix} = I_0 \begin{pmatrix} \beta_{15} e_1 e_3^* \\ \beta_{15} e_2 e_3^* \\ \beta_{31} e_1 e_1^* + \beta_{31} e_2 e_2^* + \beta_{33} e_3 e_3^* \end{pmatrix} \qquad [S5.5]$$

According to the experimental arrangement used in which we have measured J_z, for simplicity we limit the derivation only at one specific case: in-plane incidence, that is $\theta = 90°$.

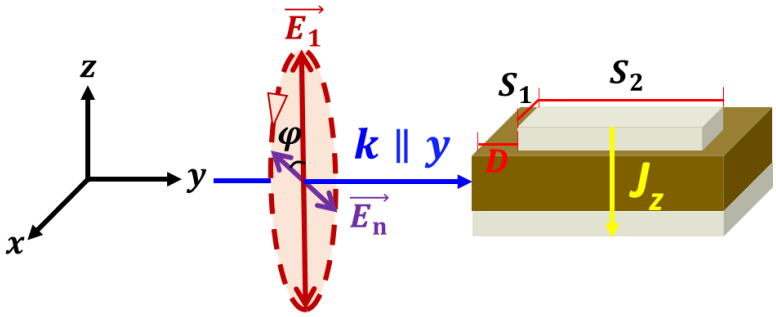

FIG. S5.2. Sketch of the experimental arrangement used to measure the photocurrent along the z-axis, when the sample is illuminated in-plane ($\boldsymbol{k}//\boldsymbol{y}$; θ = 90°) and the profile (decay) of light intensity. The length of the top electrode (S_1 x S_2) along the propagation direction of light is S_2; the gap between the crystal lateral surface and the top electrode is D << 1 μm.

According to Eqs. [S5.2, S5.4], the electric field of the light propagating along $\boldsymbol{k}//\boldsymbol{y}$ is:

$$\overrightarrow{E_{k\|y}} = |E_0|\left[\overrightarrow{e_x}\sin\varphi\, \mathrm{e}^{-\left(\frac{\alpha_\perp y}{2}\right)}\mathrm{e}^{\mathrm{i}(ky-\omega t)} + \overrightarrow{e_z}\cos\varphi\, \mathrm{e}^{-\left(\frac{\alpha_\| y}{2}\right)}\mathrm{e}^{\mathrm{i}(ky-\omega t)}\right] \quad \text{[S5.6a]}$$

$$\equiv |E_0|[\overrightarrow{e_x}e_1 + \overrightarrow{e_z}e_3] \quad \text{[S5.6b]}$$

By Eqs. [S5.5, S5.6], the current density produced by photoabsorption in a differential volume $dxdydz$ is [10]:

$$J'_z = I_0(\beta_{31}e_1e_1^* + \beta_{33}e_3e_3^*) = I_0\left[\beta_{31}\sin^2\varphi\, \mathrm{e}^{-(\alpha_\perp y)} + \beta_{33}\cos\varphi\, \mathrm{e}^{-(\alpha_\| y)}\right] \quad \text{[S5.7]}$$

The current through a differential area *dxdy* is:

$$I'_z = J'_z\, dxdy$$

In our experimental setup, the electrode widths S_1 ≈ 450 μm and 770 μm of Cry-2 and Cry-3 (in the manuscript) are bigger than the spot diameter S_d ≈ 280 μm, thus the interval of integration along *dx* should be [0, S_d]. The total current through the lateral face S_1t is:

$$I_z = I_0\int_{0,0}^{x=S_\mathrm{d},y=S_2} J'_z\, dxdy$$

Assuming that the electrode is at the sample edge (D ≈ 0), the current density is:

$$J_z = \frac{I_0\int_{0,0}^{x=S_\mathrm{d},y=S_2}\left[\beta_{31}\sin^2\varphi\, \mathrm{e}^{-(\alpha_\perp y)} + \beta_{33}\cos^2\varphi\, \mathrm{e}^{-(\alpha_\| y)}\right]dxdy}{S_1\cdot S_2}$$

$$= \frac{I_0}{2S_2}\cdot\frac{S_\mathrm{d}}{S_1}\left\{\left[\beta_{33}\frac{1-\mathrm{e}^{-(\alpha_\| S_2)}}{\alpha_\|} - \beta_{31}\frac{1-\mathrm{e}^{-(\alpha_\perp S_2)}}{\alpha_\perp}\right]\cos2\varphi + \left[\beta_{33}\frac{1-\mathrm{e}^{-(\alpha_\| S_2)}}{\alpha_\|} + \beta_{31}\frac{1-\mathrm{e}^{-(\alpha_\perp S_2)}}{\alpha_\perp}\right]\right\} \quad \text{[S5.8]}$$

In the limit of large electrodes: $\alpha_\| S_2$ >> 1 and $\alpha_\perp S_2$ >> 1:

$$J_z = \frac{I_0}{2S_2}\cdot\frac{S_\mathrm{d}}{S_1}\left\{\left[\beta_{33}\frac{1}{\alpha_\|} - \beta_{31}\frac{1}{\alpha_\perp}\right]\cos2\varphi + \left[\beta_{33}\frac{1}{\alpha_\|} + \beta_{31}\frac{1}{\alpha_\perp}\right]\right\}$$

$$= \frac{I_0}{2S_2}\cdot\frac{S_\mathrm{d}}{S_1}[(G_{33}-G_{31})\cos2\varphi + (G_{33}+G_{31})] \quad \text{[S5.9]}$$

While the electrode width $S_1 = S_2$ ≈ 59 μm of Cry-4 (in Supplemental Material S-4) is smaller than S_d ≈ 280 μm, thus the interval of integration along *dx* should be [0, S_1] and Eq. [S5.9] becomes:

$$J_z = \frac{I_0\int_{0,0}^{x=S_1,y=S_2}\left[\beta_{31}\sin^2\varphi\, \mathrm{e}^{-(\alpha_\perp y)} + \beta_{33}\cos^2\varphi\, \mathrm{e}^{-(\alpha_\| y)}\right]dxdy}{S_1\cdot S_2}$$

$$= \frac{I_0}{2S_2}[(G_{33}-G_{31})\cos2\varphi + (G_{33}+G_{31})] \quad \text{[S5.10]}$$

Note: In Eq. [S5.9] the size of the electrode appears explicitly at the denominator.

S-6. The contribution of drift and bulk photovoltaic effect

The upper limits of $J_{BPE}(\theta, \varphi)$ (or alternatively the upper limits of BPE G_{ij} indicated in the manuscript Table I) can be obtained by assuming $J_{drift,NSW} = 0$. Notice that as oscillations of J_{sc} are well visible (G_{33} - G_{31}) and thus J_{BPE} cannot be zero. Therefore, by assuming $G_{31} = 0$, the lower bounds of $J_{BPE}(\theta, \varphi)$ can be derived from the amplitudes of J_{sc} oscillations (Figs. 2, 3 and 5).

Therefore, at 405 nm, the correlation of the three contributions in $J_{sc}(\theta, \varphi = 0°)$ can be deduced as below:

θ	$J_{drift,NSW}$ (mA/cm^2)	J_{BPE} (mA/cm^2)	$(J_{drift.NSW})/J_{sc}$	J_{BPE}/J_{sc}
0°	0 - 8.72	0 - 8.72	0 - 100 %	0 - 100 %
22.5°	0 - 8.72	0.44 - 9.16	0 - 95.2 %	4.8 % - 100 %
45°	0 - 8.72	1.52 - 10.24	0 - 85.2 %	14.8 % - 100 %
60°	0 - 8.72	2.27 - 10.99	0 - 79.3 %	20.7 % - 100 %
90°	0 - 0.029	0.015 - 0.044	0 - 65.9 %	34.1 % - 100 %

References

[1] S. H. Skjærvø, E. T. Wefring, S. K. Nesdal, N. H. Gaukås, G. H. Olsen, J. Glaum, T. Tybell, and S. M. Selbach, Interstitial Oxygen as a Source of P-Type Conductivity in Hexagonal Manganites, Nat. Commun. **7**, 13745 (2016).